Multiscale Wavelet-Based Analysis and Characterization of Fretting Fatigue Damage in Titanium Alloys

George N. Frantziskonis[1] and Theodore E. Matikas[2,*]

[1]*Department of Civil Engineering & Engineering Mechanics, University of Arizona, Tucson, AZ 85721, USA*
[2]*Department of Materials Engineering, University of Ioannina, University Campus, 45110 Ioannina, Greece*

Wavelet analysis is used to rationalize information at various scales in several branches of science, including particle physics, biology, electrical engineering, fluid mechanics, and medicine. However, this powerful technique has not been applied extensively to characterize structures of materials, fretting damage for the present case, even though many critical questions could be addressed. In particular, the following unsolved problems are considered in this paper: (a) The first problem deals with the quantitative characterization of fretted surfaces in a Ti-6Al-4V alloy. This is investigated by analyzing profilometric digital images of fretted surfaces obtained in a range of magnifications. Wavelet analysis of the data is able to identify, by examining the wavelet coefficients, dominant length scales as those regions in scale-space where the energy of the wavelet transform and/or peaks of local concentration dominate. For the range of magnifications examined, i.e. from $1.25\times$ to $100\times$, the $\sim 20\times$ magnification is identified as the one with the most useful information. (b) An alternative procedure is employed for the second use of wavelets which deals with the non-uniformity of the contact regions. Wavelet analysis is employed to identify partially slipping regions, which result in the "pattern" of the fretted surface morphology.   [doi:10.2320/matertrans.MRA2008378]

1. Introduction

Load transmission is very often attained by contact, as is the case in the problem of fretting damage. In this situation, contact arises over a macroscopically flat surface, with a radius of curvature at the edges, usually pre-existing or generated by wear. The design process for these contacts is usually derived from experience, and it is very difficult to examine the details of the contact during fatigue, and the transition to fretting damage. A large part of practical analysis is rather *post-mortem*, where the fretted surfaces are examined. Since fretting damage is progressive, an important problem is to decide the magnification to use for examination of the fretted surfaces. Under present and current practices, tests on fretting are done at a single magnification, which is decided arbitrarily or empirically. Thus, only features at that magnification are seen. Whether features at other magnifications prove to be more important is not addressed under such practice. It is, partly, the aim of this work to identify fretting fatigue issues at different magnifications and whether there exists an optimum magnification to be used in practice. An optimum magnification would yield the most useful information, and pave the road towards better understanding of fretting.

The contact surfaces in the fretting problem are macroscopically flat, and usually analysis is performed under this "assumption". However, surface undulations exist at several scales, and the relevant "pattern" is highly scale dependent. Identifying the morphology of such undulations, at several spatial scales, provides information on the morphology of the partially slipping regions, and those with sticking contact or no contact at all. This work addresses both issues above using the powerful tool of wavelet analysis.

It is not attempted to provide a review of the rather extensive literature on fretting, yet reference is given to these efforts which are directly related to the present study; reviews can be found in.[1–3] The aim of this paper is to: (a) identify those magnifications under which the most useful information on fretted surfaces is obtained; (b) identify the "pattern" of the partially slipping regions, as opposed to the sticking ones, during surface-to-surface contact and correlate it with actual fretted surface patterns. Wavelets are used herein due to their elegant multiresolution properties which allow them to serve as a multiscaling tool to study fretting fatigue damage as a multiscale phenomenon. Wavelets are particularly well-suited as a tool to study the effect of magnification used in studying fretting. The following section provides a brief introduction to wavelet analysis and is followed by the description of the performed experiments and the wavelet analysis of the data.

2. Wavelet Analysis—Background

The wavelet transform can be seen as a mathematical microscope: when increasing the magnification, one gains insight into the intricate structure of a "pattern". Wavelets provide a mean to mathematically represent functions of space and/or time- and scale-wise with a few parameters. The so-called wavelet coefficients provide local information on the function and also information relevant to scale (level of magnification in space/time). Fourier transforms based on combinations of sines and cosines are very useful for describing periodic and stationary functions, but they cannot describe nonperiodic, nonstationary phenomena encountered in the physical world. Hence, the use of wavelets has found riches in analyzing complex signals and structures.

Let us briefly present an illustrative example of use of the wavelet transform, for the purpose of further understanding and facilitating the subsequent description of the present work. Figure 1 shows a digital image (512×512 pixels) of a polycrystalline structure that resulted from Molecular Dynamics simulations (Figs. 1 to 3 are from work published
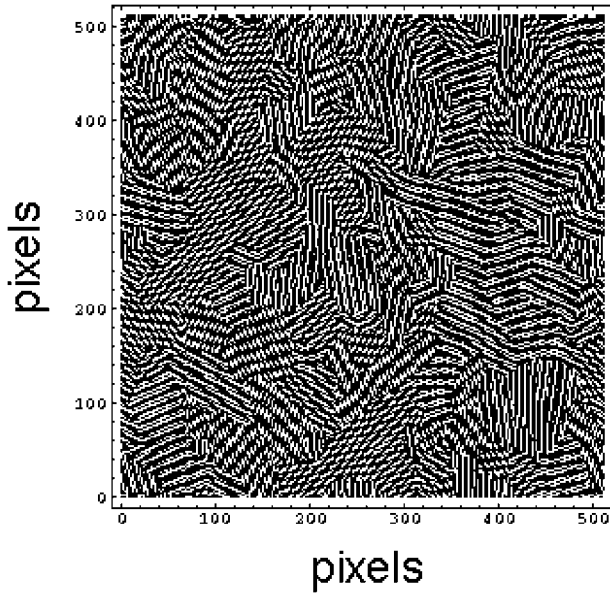
*Corresponding author, E-mail: matikas@otenet.gr

Fig. 1 A digital image of a material microstructure. The image is a result of MD simulations as described in the text.
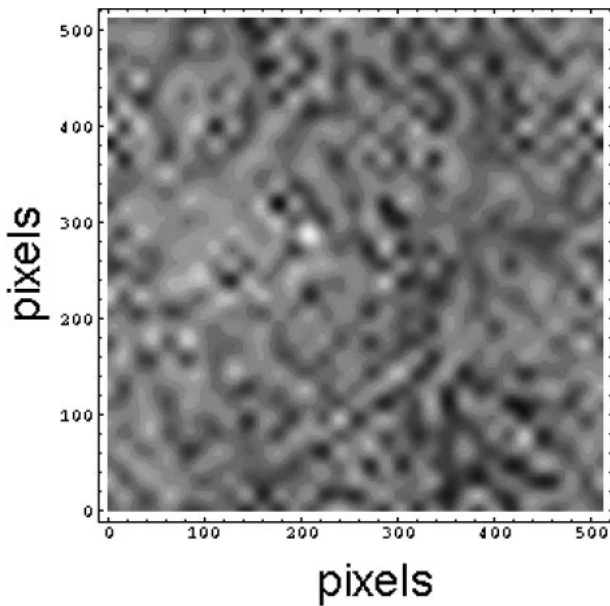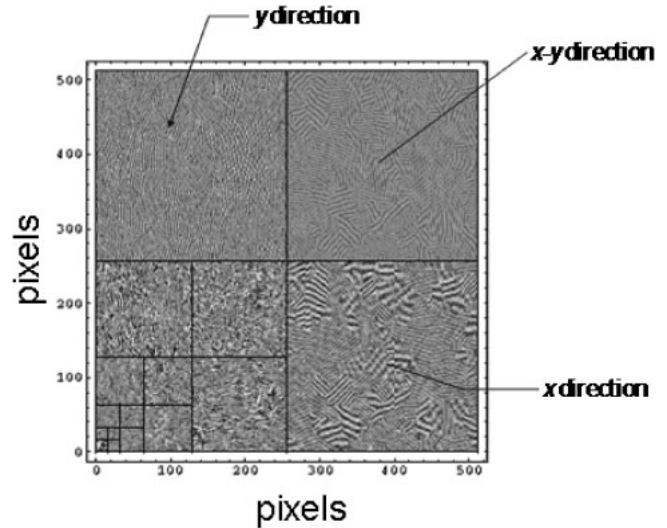

Fig. 3 The wavelet transform of Fig. 1 where all the decomposition images have been arranged in a large matrix equal to the size of Fig. 1. Details of the arrangement are shown for the finest decomposition (three 256×256 images).

Fig. 2 The wavelet representation of the Fig. 1 at resolution 32 times coarser than the original.

in Ref. 4)). The microstructure was obtained from solidification of a melt; the solid microstructure was subsequently annealed for one hour. Figure 2 shows the wavelet representation (not the wavelet transform, as explained later) of the image at a resolution 32 times coarser than that of the original image. In other words, it shows the structure of the polycrystalline material as observed with a magnification 32 times coarser than the detailed image (Fig. 1). The wavelet representation provides spectacular evidence of its capability to describe spatial "patterns" at different scales realized as magnifications; Fig. 2 illustrates the spatial pattern of the material for a coarser value of the magnification. In the present work, instead of the material structure, fretted and unfretted surfaces are analyzed.

A more general goal of wavelet analysis is to describe graphs (signals) as superposition of elementary functions. The corresponding description is then used for different purposes, i.e. data compression, feature extraction, pattern recognition, etc. There are several publications on this relatively new subject and applications can be found in a wide variety of scientific/engineering fields, e.g.[5–15] Wavelet transforms provide both scale and location (and/or time) information about a given function. A wavelet $\psi(x)$ (with real values in our case) transforms a function $f(x)$ according to

$$W_f(a,b) = \int_\infty^\infty f(x)\psi_{a,b}(x)dx \qquad (1)$$

The two-parameter family of functions, $\psi_{a,b}(x) = (1/\sqrt{a})\psi(\frac{x-b}{a})$ is obtained from a single one, ψ, called the mother wavelet, through dilatations by the factor a^{-1} and translations by the factor b. The factor $1/\sqrt{a}$ is included for normalization purposes and, with it, all the wavelets have the same energy. The scale parameter a can take any value on the positive real axis. The scalars defined in (1) measure the fluctuations of $f(x)$ around point b at the scale a.

A wavelet analysis can either be continuous or discrete. The second one, based on an orthogonal decomposition of a signal can be performed with fast algorithms. For obtaining Fig. 2, biorthogonal symmetric wavelets of order 12,4 and the corresponding so-called scaling functions[5] were used.

Given the wavelet coefficients $W_f(a,b)$ associated to a function f, it is possible to reconstruct f in real space $f = f(x)$ through the inversion formula

$$f(x) = \frac{1}{c_\psi} \int_0^\infty \int_{-\infty}^\infty W_f(a,b)\psi_{a,b}(x)db \frac{da}{a^2} \qquad (2)$$

At any given scale $a > 0$, f is decomposed into the summation of a "trend" at scale s and of a "fluctuation" around this trend. The trend is the contribution from all scales $s > a$ in (2), and the fluctuation is given by the scales $s < a$. By choosing any desired limits for the scale parameter a we

obtain the representation of f at desired scales, e.g. that of Fig. 2.

A two-dimensional wavelet transform includes a transform in the x direction, a transform in the y direction and one in the x-y direction. For example, given an image of 512×512 pixels, the wavelet transform consists of three 256×256 images (one in the x direction, one in the y, and one in the x-y direction), three 128×128, and so on; each decomposition level is at half the resolution from the previous one. The final level of decomposition represents the image at the coarsest resolution (its size depends on the support length of the wavelets used and for example it could be an image 16×16 pixels). Figure 3 shows the wavelet transform of Fig. 1, where the matrices have been arranged into a big matrix of the size of the original data. Figure 2 was derived by performing the inverse wavelet transform using only the wavelet transform data (Fig. 3) up to the resolution 32 times coarser than that of the original image.

3.   Experimental Procedures

3.1   Fretting fatigue testing

The fretting experimental setup was designed to simulate the loading conditions under which fretting fatigue damage occurs in turbine engine blade components. This loading condition includes a normal and a shear load against the blade-disk interface, and a bending moment induced by the dovetail flank angle. The two contacting surfaces, both of Ti-6Al-4V, are flat-on-flat with blending radii on both the blade root and the disk slot. The test apparatus used in the fretting experiments simulates the blade root geometry by employing flat fretting pads, with a radius at the edge of contact, against a flat specimen as shown in Fig. 4. The gripping system of the fretting fatigue machine was designed with a set of two removable square fretting pads (25.4×25.4 mm) to facilitate control of the surface conditions and bolts instrumented with strain gages in the shank to quantify static normal loads.

The axial fretting fatigue specimen is sandwiched in the grips, the normal load is adjusted by tightening the instrumented bolts then, the mean axial and dynamic loads are applied through pneumatic control, and an oscillatory axial load is applied with an electromagnetic shaker. The specimen configuration produces two fretting fatigue tests per specimen. Fretting damage occurs near the edge of contact between the specimen and the fretting pads. In the sample that was used for this analysis, the material had been
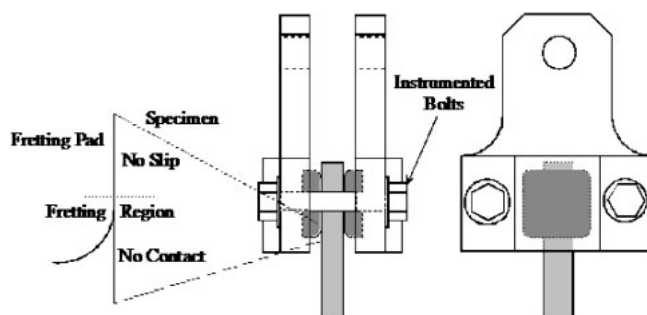
fractured on one fretting surface. The opposite end was characterized. This specimen end can be assumed to be near its fretting fatigue life.

For the experimental results presented in the following sections, the Ti-6Al-4V specimens were machine-finished and not polished. Each specimen has dimensions 10 mm in width, 2 mm in thickness and 100 mm in length. For the fretting contact, a normal stress of 302 MPa was applied. The mean axial stress was 108.8 MPa with an amplitude ratio of 0.1 applied at 250 Hz. This resulted in a fatigue life of 3.36×10^7 cycles.

3.2   Profilometry

White Light Interference Profilometry was used to measure the surface topography before and after the specimens were subjected to load. This technique is capable of a lateral surface resolution of $0.2\,\mu m$ and a vertical resolution of the height of the sample of approximately 1 nm. The profilometer operates by reflecting a white source light off of the surface of the material. The light that is reflected from the surface is combined with the light reflected off a reference surface. This surface is at a known distance from the beam splitting optic. When the light travels the same distance to the reference surface and the test surface, a fringe pattern can be seen as the height profile of the sample causes the light off of the surface to be successively in and out of phase. By scanning the vertical span of the material and recording the heights where the primary fringes (those with the highest contrast) are seen, the surface topography is recorded. This data is then expressed as a grayscale level in which black represents the lowest regions on the surface of the material while white represents the highest regions.

4.   Experimental Results

Images of the surfaces (fretted and unfretted) were acquired at magnifications ranging from $1.25\times$ to $100\times$ (1.25, 2.5, 5, 10, 20, 40, 50, 100). Figures 5 and 6 present typical $196.8\,\mu m \times 196.8\,\mu m$ images with $20\times$ magnification, showing clearly visible fretting damage; it will be demonstrated later that, for these series of tests, the $20\times$ magnification is the one containing the most useful information.

Figure 7(a) shows a $3\,mm \times 3\,mm$ image with $1.25\times$ magnification corresponding to the same sample, as the one shown in Fig. 6(b). As it can be observed, the fretted area is only concentrated in a small area. In order to locate the region where Fig. 6(b) corresponds to, the $5\times$ image is also provided (Fig. 7(b)). The small, $768\,\mu m \times 768\,\mu m$, square delineated in Fig. 7(b) indicates the region of Fig. 6(b), which corresponds to the fretted zone of the sample.

5.   Wavelet Analysis of Fretted and Unfretted Surfaces

As mentioned in the introduction, much research has been conducted on understanding the nature of fretted surfaces. However, the task of studying how information appears at various scales on a relative and comparative basis has not been undertaken. As a consequence, the question as to "which magnification(s) should be used for studying fretting
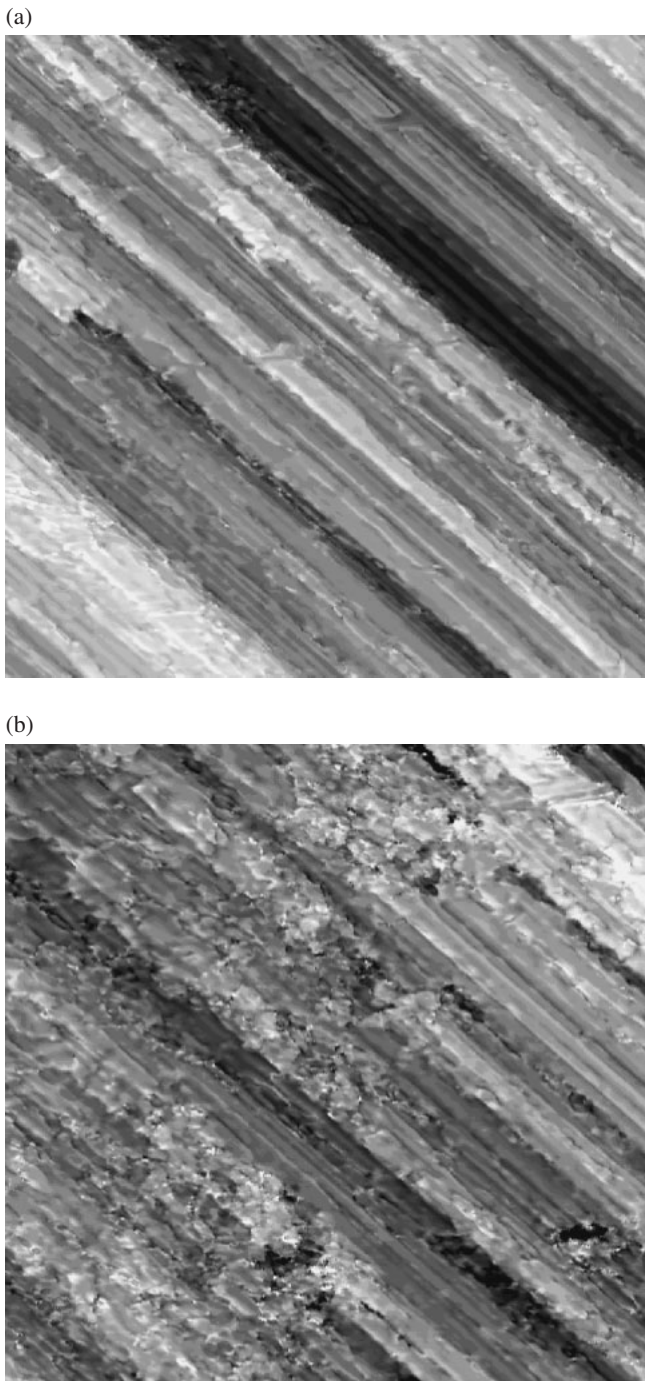

Fig. 4   Fretting fatigue gripping system.

(a)

(b)

Fig. 5 Typical images of (a) the unfretted surface and (b) the fretted surface, for specimens with machine lines oriented at ∼45° from the horizontal.
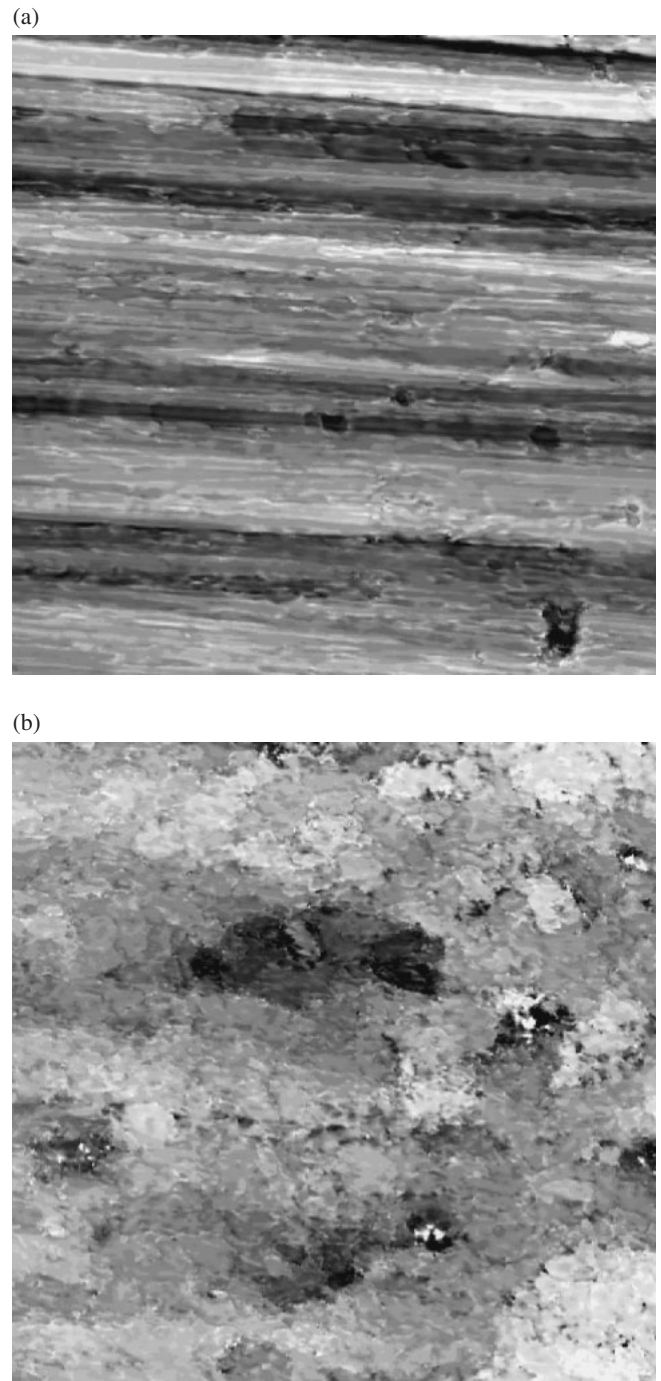
(a)

(b)

Fig. 6 Typical images of (a) the unfretted surface and (b) the fretted surface, for specimens with machine lines oriented at ∼5° from the horizontal.

fatigue" is frequently left unanswered. We address this important issue, along with the reasons of why wavelet analysis is ideal for identifying dominant scales.

Using wavelet analysis, we studied the fretted and unfretted surfaces at magnification increases from $1.25\times$ to $2.5\times$, $2.5\times$ to $5\times$, etc. In other words, since data at several magnifications is available, the wavelet synthesis of the data (as opposed to wavelet decomposition) can be performed, as done in Refs. 4, 16, 17) for various other problems for example. This is done by performing the wavelet transform for the $100\times$ images, for example, and studying the wavelet coefficients that represent the details from $50\times$ to $100\times$. Each wavelet coefficient corresponds to a specific spatial position in the image and to a specific scale of details, and it indicates the sharpness of the variation (surface height for the present case) in the image at that spatial location and scale of details. In other words, the higher the absolute value of a wavelet coefficient the sharper the variation at the corresponding location and corresponding scale. This powerful analysis reveals the heterogeneity in the surface structure in a multi-resolution fashion, so we can reveal details at several scales concurrently.
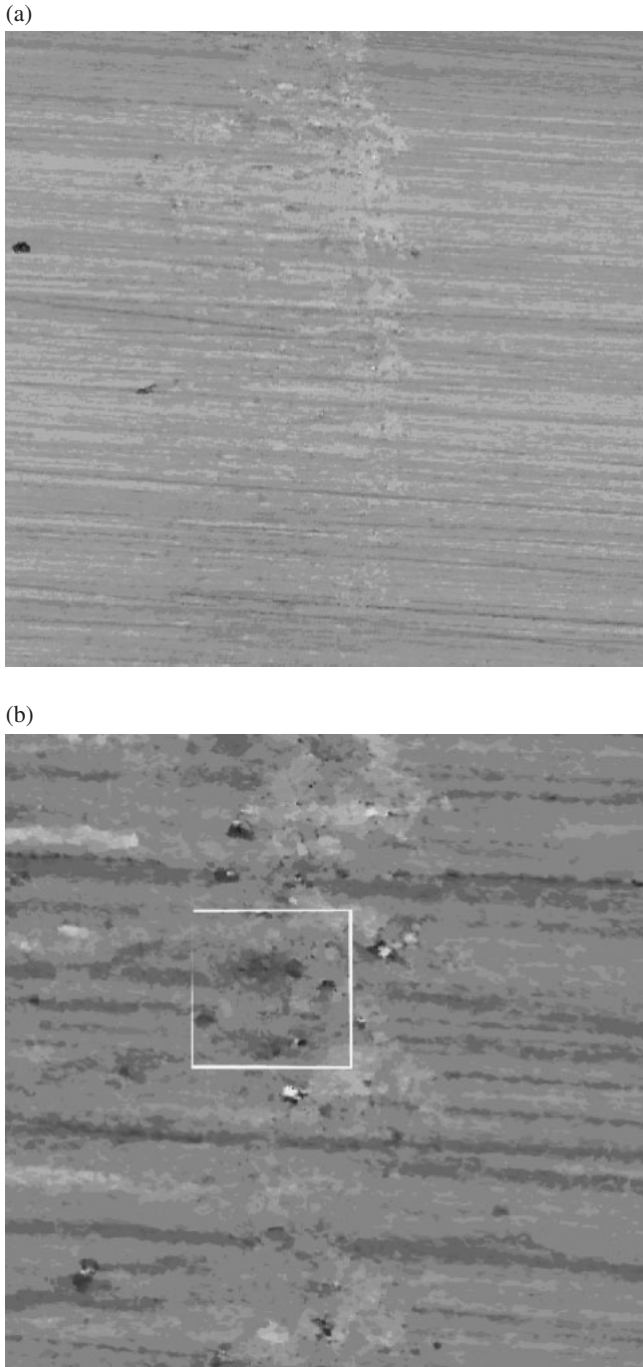
(a)

(b)

Fig. 7   (a) $1.25\times$ magnification image for the same sample as that shown in Fig. 6(b). (b) $5\times$ magnification image for the same sample as that shown in Fig. 6(b). The square indicates the small region where Fig. 6(b) is located.

Since we have surface height data at several magnifications, we can study the details from one scale to the next. Before presenting the results of the analysis, it is worth repeating, see previous section, that for one set of images with magnifications of $1.25\times, 2.5\times, 5\times, 10\times, 20\times$, and $40\times$ the final machining lines are at about $5°$ inclined to the horizontal axis—i.e. the direction of the cyclic stress—while for another set of $10\times, 20\times, 40\times, 50\times$, and $100\times$, the machining lines are at about $45°$. In a preferred environment, a large number of angles between machine line and the horizontal axis should be examined. However, this is difficult
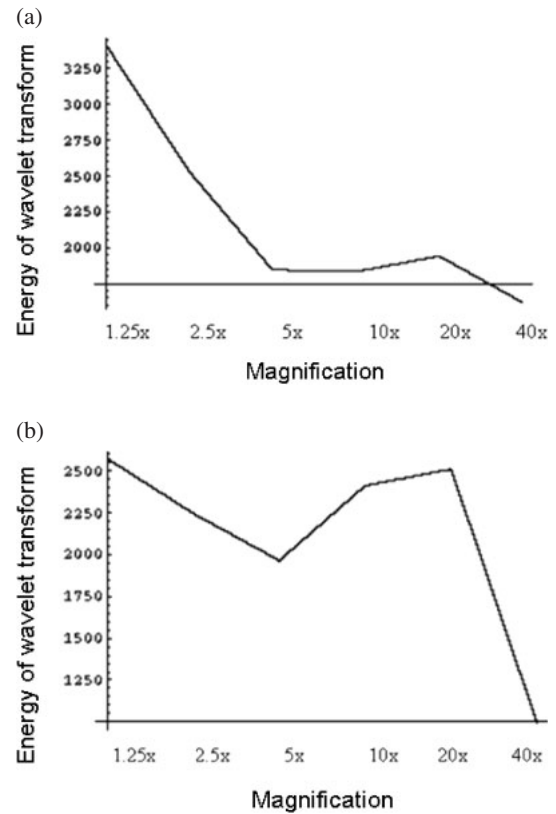
(a)

(b)

Fig. 8   The energy of the wavelet transform, the part representing the details from coarser scales, from the first set of images. The horizontal axes represent the level of magnification and the vertical the energy of the transform for (a) unfretted surfaces; (b) fretted surfaces.

to achieve experimentally, thus two angles, a small $(5°)$ and one between $0°$ and $90°$ $(45°)$ were chosen.

Figure 8 shows the wavelet coefficients (in particular the energy of the wavelet transform, defined in a "signal processing" sense as the dot product of the matrix of coefficients with itself) that represent the details from coarser scales for images of the first set of images (machine lines at about $5°$ to the horizontal) and similarly Fig. 9 for the second set (machine lines at about $45°$ to the horizontal). From these results we can deduce the following:

The wavelet coefficients representing the details from coarse to fine scales, and for the unfretted surfaces the details (energy of the transform) decreases with increasing magnification. However, for the fretted surfaces the energy of the transform at $20\times$ increases significantly (relative comparison with the fretted surfaces). Thus, the most important scale is revealed at $\sim 20\times$, and other scales are of decreasing importance for fretted surfaces. This implies that at $20\times$ the fretted surface contains the most useful information or $20\times$ shows maximum "tortuous" or least flat features, which depict the extent of fretting damage. Obviously, we have only examined a single "realization" of the surfaces; a statistical treatment is more applicable here, and this as well as other important issues are now addressed. Of course, other materials have to be tested accordingly to find the magnification with most useful information. There should be a relation between the size of material features (e.g. grain size) and information at various magnifications, yet that relation is not addressed herein.
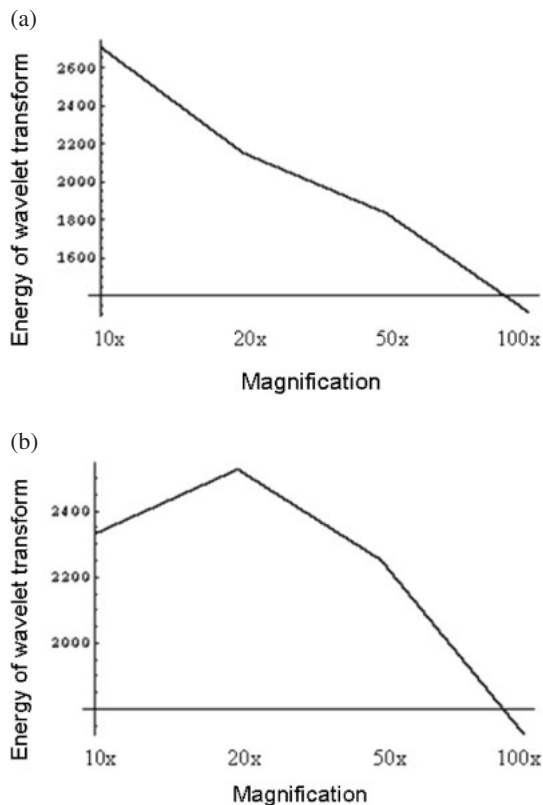
(a)

(b)

Fig. 9 The energy of the wavelet transform, the part representing the details from coarser scales, from the second set of images. The horizontal axes represent the level of magnification and the vertical the energy of the transform for (a) unfretted surfaces; (b) fretted surfaces.

We only considered magnifications from $1.25\times$ to $100\times$. At finer scales there may be other surface features that may prove important. Thus, this work is amenable to using higher magnifications, up to $150,000\times$, through SEM and TEM in addition to optical microscopy. Since our findings show that the length scale revealed by wavelet analysis at $20\times$ is important, we now focus at this scale. Before we present the analysis of images at $20\times$, we discuss the process used.

Since we have to deal with studying subsets instead of entire populations, then a relatively large field of observation (with respect to the features observed) requires only a small number of samples (assuming ergodicity), while the opposite is true for a small field of observation. Each micrograph represents an image with gray scale spatial variations (which represent variations in surface height), so data at each scale is obtainable through identifying appropriate spatial correlation functions for the corresponding wavelet coefficients. This is important since obtaining very large images, difficult to acquire and process numerically, is avoided. Properties of the micrograph can be read from properties of their wavelet transform and *vice-versa*. Thus, mathematical metrics of structure at each scale can be obtained. Such a statistical analysis appears in the appendices—this is important for the study of surface undulations presented in the sequence. Based on the analysis it is revealed that the unfretted surfaces have surface undulations at all scales, in a more "regular" fashion in the direction transverse to the machine lines rather than parallel to them. Thus contact should be studied in a multiscale fashion.

6. Effects of Surface Condition

It is interesting to study whether the surface undulations, responsible for partially slipping contact areas, can be picked up efficiently at some specific scale, or detail space from one scale to another. In relevant developments,[18,19] it has been shown that in a contact problem with constant normal load, the partially slipping zones remain the same as those activated during the normal loading process. This, then, indicates that the pattern of the fretted zones are "decided" before the tangential load is applied. This pattern depends solely on the geometry of the contacting surfaces, and on the magnitude of the normal applied load. The influence of the geometry of the contacting surfaces on fretting has been studied both experimentally and theoretically.[20–23] The conclusion of these studies is that as surface roughness increases fretting resistance also increases. The roughness of surfaces restricts the actual contact to a number of small areas at the peaks of the surface asperities. As the normal load is increased, these asperities deform, allowing the solids to move closer together and causing more contact areas to be formed. Thus, the contact of sliding solids is restricted to a number of small areas. However, in this case the distortion produced by the relative motion of the solids will cause the actual contact areas either to be transient due to the fracture of the junctions, or to more relative to one or both solids.

Unfortunately, it is extremely difficult, if not practically impossible, to have the image (at $20\times$) of the fretted region before fretting. Thus we have to examine images of fretted and unfretted regions from different locations. This can be done efficiently by studying the statistics of the wavelet coefficients for the fretted and unfretted surfaces. Such a study, along the lines of Appendix A, has yielded that the coefficients at the detail scale for the scales shown in Figs. 10 and 11, in the direction of fretting, i.e. the horizontal one, are statistically similar. As can be seen also from Figs. 10 and 11, the representation of the surfaces at these details are also similar (optically), and the ones representing the fretted surfaces capture the morphology of the fretting "pattern".

It is worth noting that this detail space, i.e., from $2.5\times$ to $5\times$, was the one at which the wavelet coefficients show the strongest statistical similarity, and also the images of fretted and unfretted surfaces showed optical similarity. In other words, the present study reveals that surface undulations at such scales are important for the contact problem. Thus by modifying these undulations, e.g. mechanically, resistance to fretting will be modified. Before elaborating on this further, we present results for fretting on polished surfaces.

Experiments similar to the ones described above were performed using the same setup and materials, except that the surface of the specimen was polished to a smooth surface. The normal stress used in the experiment was 551 MPa. The sample was fatigued under a mean axial stress of 195 MPa with a stress amplitude ratio of 0.1 at 250 Hz for 8.98×10^5 cycles, at which time fretting fatigue failure occurred.

The absence of machine lines changed the fretting process rather dramatically. Here, fretting damage could only be
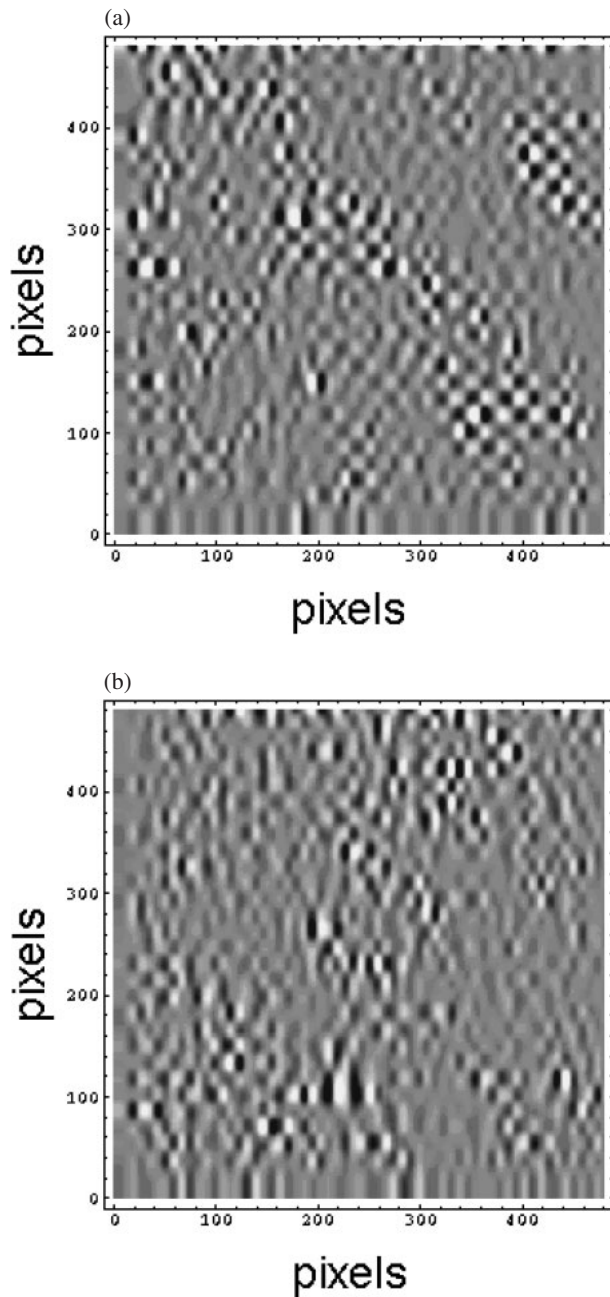
(a)

(b)

Fig. 10   Representation of (a) the unfretted surface and (b) the fretted surface for one test series (machine lines oriented at ~45° in relation to the horizontal) for the detail space 1.25×. The images were obtained through the wavelet coefficients from the transform of the images at 20×.
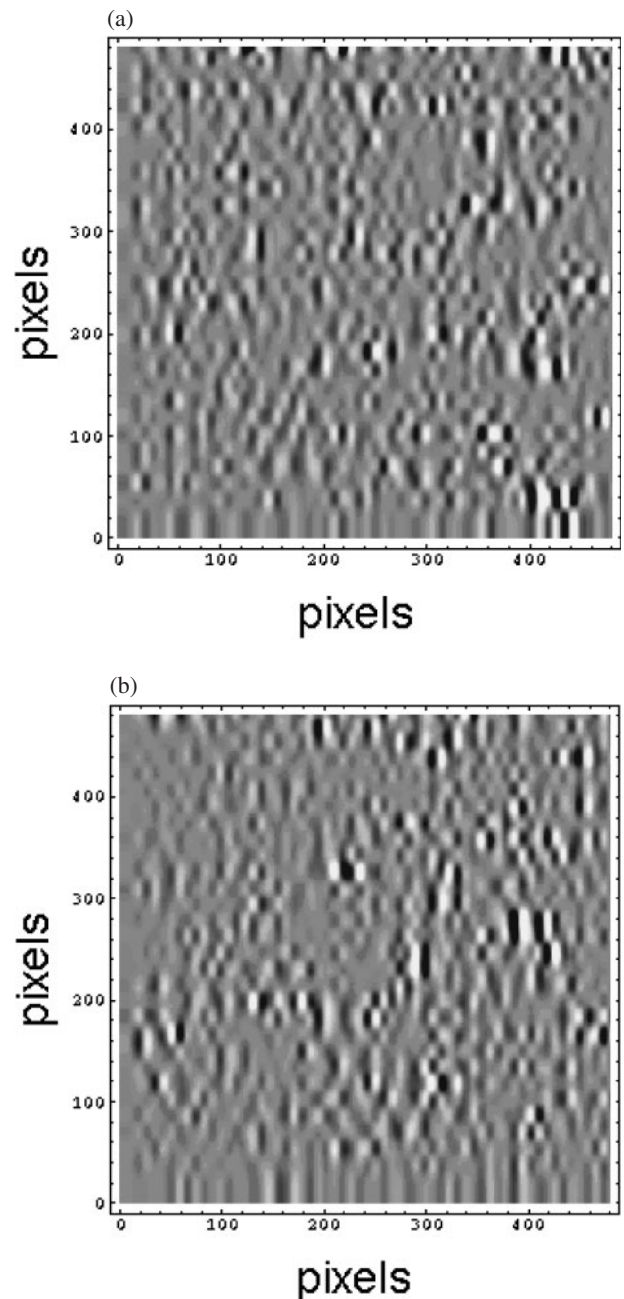
(a)

(b)

Fig. 11   Representation of (a) the unfretted surface and (b) the fretted surface for another test series (machine lines oriented at ~45° in relation to the horizontal) for the detail space from 2.5× to 5×. The images were obtained through the wavelet coefficients from the transform of the images at 20×.

observed at high magnifications (much higher than the ones used for fretting damage in machined specimens). Figure 12 shows a SEM image of the fretting damage at approximately 2000× magnification.

Since profilometry at such high magnifications is not easy (the available atomic force microscope could provide such data but for a small area, and this is not adequate for the purposes herein) at this stage we are not able to identify dominant scales as was the case for the machined specimens. We are presently attempting to do such a study based on SEM images, yet there are several issues to be resolved. However, profilometry at lower magnifications is able to provide useful information. Figure 13 shows the profilometric image of the

unfretted surface at 40× magnification. This clearly shows that even though roughness (in the "traditional" sense of the word) of the polished surface appears at very small scales, surface undulations at larger scales is appreciable and important for fretting.

Appendix B presents an analysis of this image along the lines of Appendix A. Since the profilometric image of the fretted surface (at 2000×) is not available, a wavelet based comparative study (fretted versus unfretted), as was done for the machined surfaces, is not feasible at this stage. Yet, Fig. 14 shows the wavelet representation of the image of Fig. 13, for the detail space from 1.25× to 2.5×. Although

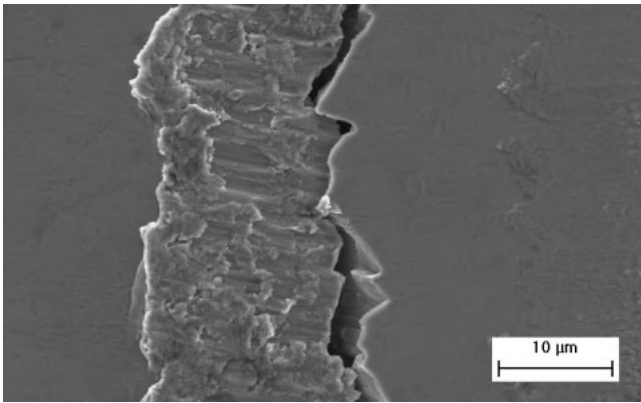Fig. 12   A SEM image of the fretting region at about 2000× magnification.

Fig. 14   Representation of the unfretted surface (Fig. 13) for the detail space from 1.25× to 2.5×. The image was obtained through the wavelet coefficients from the transform in the horizontal direction of the image of Fig. 13.
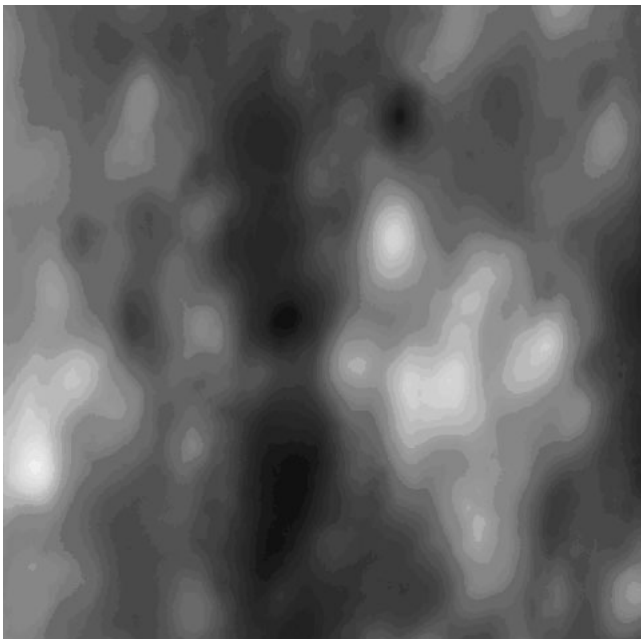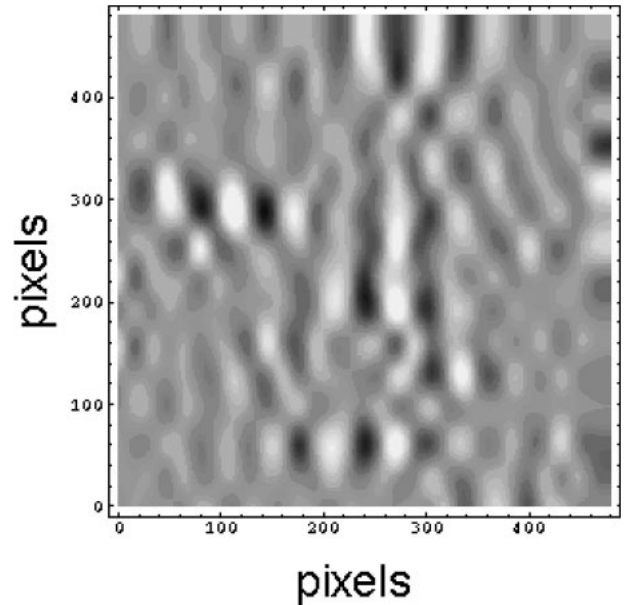

Fig. 13   Image from profilometry of the unfretted surface at 40× magnification. The image is 100 μm × 100 μm; the maximum height difference is 86 nm.

statistical comparison with the fretted surfaces is not directly feasible at this stage, the "pattern" of this image can be related to the fretting pattern.

7.   Conclusions

The wavelet analysis allows a multiscale description of the morphology of fretted and unfretted surfaces. Thus, one is able to compare information obtained at different scales, and identify the scale (or range of scales) where information is most useful. Furthermore, the surface morphology at several scales is important for fretting damage; for machined surfaces, undulations at scales higher than that of the machine lines prove important. Thus, alteration of such undulations in an optimum way will lead to improved resistance to damage. Similar conclusions hold for the polished surfaces, though further experimental data at higher magnifications will provide more insight. This work is amendable to incorporating other effects in addition to the

geometrical ones, e.g. material microstructure and its relation to the surface morphology, temperature fields during fretting, etc. Yet, the present work paves the way towards multiscale analysis of experimental data. According to the present study, a multiscale approach would not be necessary for the following two cases, not realizable in practice: (a) the surface is flat at all scales; (b) the surface possesses perfect self-similarity (fractal) at all scales, i.e. there are no upper or lower cutoffs, there are no deviations from perfect self-similarity, etc.

Acknowledgements

Appendix A: Statistical analysis of the unfretted machine-finished surfaces

Useful information on the statistical properties of the unfretted surfaces can be obtained by studying the spatial correlations. A "standard" analysis[24,25] calls for studying the so-called variance of increments V defined as

$$V = \langle |h(\vec{x}) - h(\vec{x} + \vec{r})|^2 \rangle \qquad (\text{A·1})$$

where h denotes the surface height as a function of position $\vec{x}$, and $\langle . \rangle$ indicates expected value. Figure A·1 shows V for the unfretted surface with the machine lines $\sim 5°$ to the horizontal.
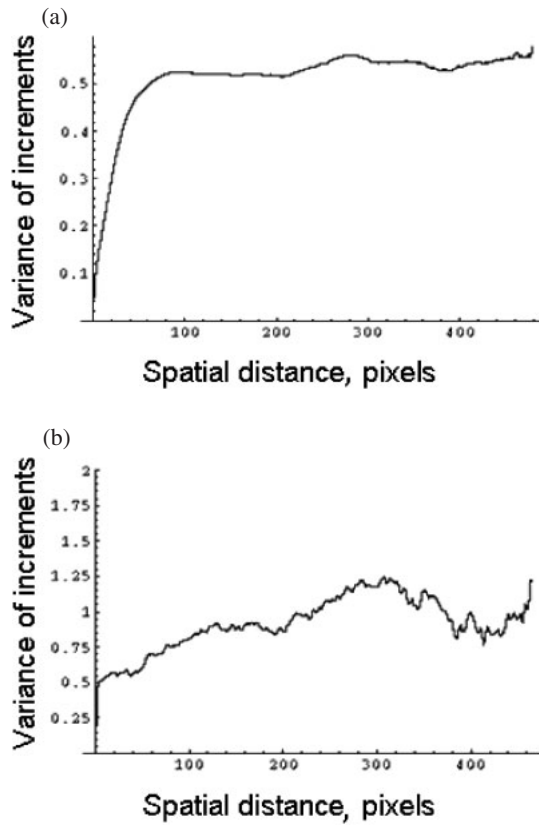
(a)

(b)

Fig. A·1   Variance of increments V in μm^2, vertical axes, as a function of spatial distance r one unit/pixel $= 6.23\,\mu m$, horizontal axes, for the unfretted surfaces with the machine lines $\sim 5°$ from the horizontal obtained from the $1.25\times$ magnification image. (a) In the vertical direction; (b) horizontal direction.

(a)

(b)

Fig. A·2   Log-log plot of scale a, horizontal axes, versus M_a, vertical axes for the unfretted surfaces with the machine lines $\sim 5°$ from the horizontal obtained from the $1.25\times$ magnification image. (a) in the vertical direction; (b) in the horizontal direction.

As can be seen the surface is stationary, i.e. the value of V does not increase indefinetely with r. In the vertical direction a variance of $\sim 0.5\,\mu m^2$ can be identified and a correlation distance of ~ 80 pixels or $80 \times 6.23 \cong 500\,\mu m$. In the horizontal direction a clear plateau is not reached, yet a sharp increase in V is observed for small spatial distances. Thus a clear correlation distance and variance in the horizontal direction (the direction of fretting in this case) cannot be identified. Thus statistical information in the horizontal direction os highly scale-dependent, and this justifies further the wavelet-based study of the surfaces.

In a relevant work[26] a very efficient method for studying the properties of a surface scale-wise (and for determination of the Hurst exponent, for self-affine surfaces) was introduced and examined in detail. The method, based on wavelet analysis of data, is clearly shown to outperform other methods available, especially when a few number of samples or even single realizations are available. The method is based on studying the wavelet coefficients at each scale of decomposition, and in particular studying

$$M_a = \langle |W[h](a, b)| \rangle_b \qquad (A\cdot 2)$$

i.e., the spatial expected value (b denotes space variable) of the wavelet coefficients of a function h for each scale a. As shown, when a function $h(x)$ scales, in a statistical sense, such that
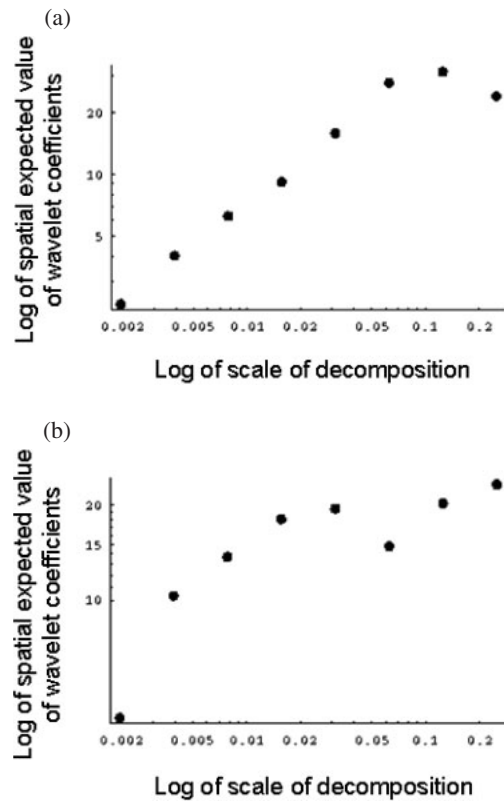
$$h(x) = \lambda^{-H} h(\lambda x) \qquad (A\cdot 3)$$

then its wavelet transform satisfies

$$W[h](\lambda a, \lambda b) = \lambda^{H + \frac{1}{2}} W[h](a, b) \qquad (A\cdot 4)$$

In the case $0 < H < 1$, function h is self-affine. By averaging out the dependency on the translation parameter a, i.e., by calculating, for each scale of decomposition a, M_a and by plotting, in log-log plot, a versus M_a, the slope of the straight line is $1/2 + H$. Of course, since data in this case (surface geometry) are two-dimensional, we get a slope for two perpendicular directions, i.e. x and y. Different H in the two directions implies anisotropy. Note that H can depend on scale a implying different properties at different scales, e.g. self-affinity at certain scales, statistical stationarity at other scales, etc.

Figure A·2 shows the log-log plots of a versus M_a for an unfretted surface. It can be seen that in the vertical direction (Fig. A·2(a)) for large scales the surface becomes stationary (slope of the curve becomes zero and subsequently negative) while in the horizontal direction (Fig. A·2(b)) the "disorder" of the surface is highly scale-dependent.

Figure A·3 is similar to Fig. A·2 but for another image of the surface. Comparing Figs. A·2 and A·3, it can be revealed that the unfretted surfaces have surface undalations at all scales, in a more "regular" fashion in the direction transverse to the machine lines rather than parallel to them.
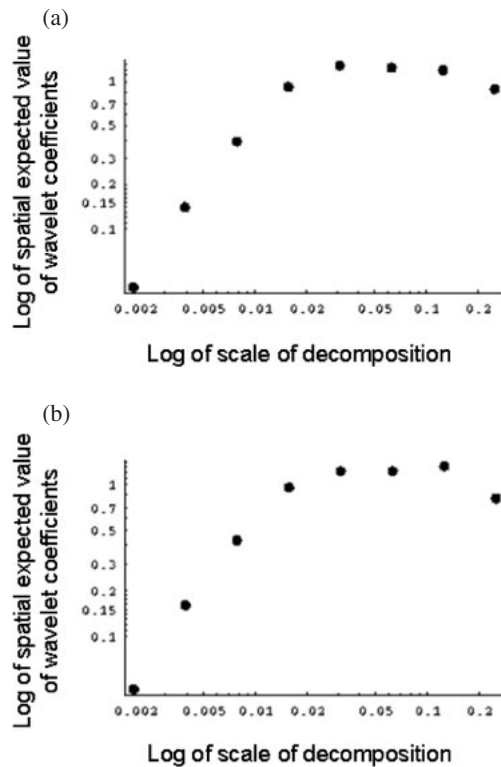
(a)

(b)

Fig. A·3   Log-log plot of scale a, horizontal axes, versus M_a, verical axes for the unfretted surfaces with the machine lines $\sim$45° from the horizontal obtained from the 5× magnification image. (a) in the vertical direction; (b) in the horizontal direction.

Appendix B: Analysis of the unfretted polished surfaces

A process similar to that shown in Appendix A was applied for the polished surfaces. Figure B·1 shows the log-log plots of a versus M_a for an unfretted polished surface, obtained from the image of Fig. 14.

It can clearly be observed that the surface undulations are multiscale, i.e. the slope of the graph changes with the scale. Correlation analysis did not show any trend, nor it reached a plateau, which would indicate the existense of a particular correlation distance.

REFERENCES

1) R. B. Waterhouse: Fretting Fatigue Int. Mater. Rev. **37** (1992) 77–97.
2) D. A. Hills and D. Nowell: *Mechanics of Fretting Fatigue*, (Kluwer Academic Publishers, Dordrecht, The Netherlands, 1994).
3) J. R. Barber and M. Ciavarella: Int. J. Solids Structures **37** (2000) 29–43.
4) G. Frantziskonis and P. Deymier: Mater. Sci. Eng. **8** (2000) 649–664.
5) D. Lokenath: *Wavelet Transforms and Their Applications*, (Birkhauser Publ., 2001).
6) M. B. Ruskai, G. Beylkin, R. Coifman, I. Daubechies, S. G. Mallat, Y. Meyer and L. Raphael ed.: *Wavelets and their Applications*, (Jones and Bartlett Publ., Boston, 1992).
7) Y. Meyer and S. Roques ed.: *Wavelet analysis and applications*, (Editions Frontires, Singapore, 1993).
8) H. Tian-Xiao: *Wavelet Analysis and Multiresolution Methods*, (CRC Press, Boca Raton, Florida, 2000).
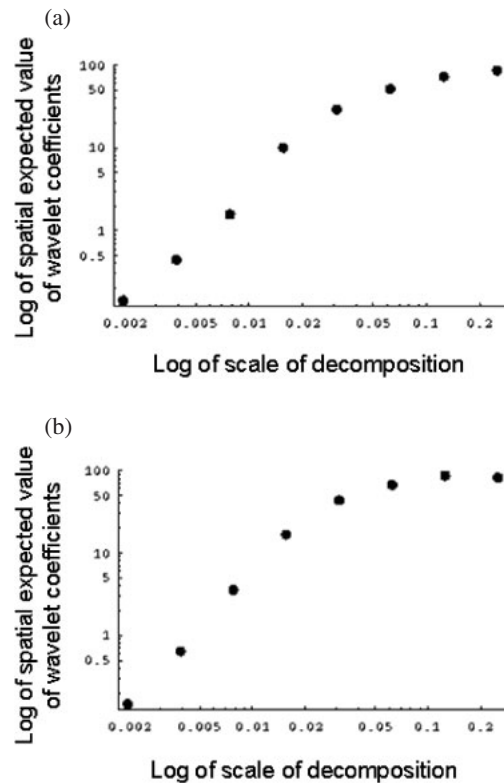9) D. S. Forsyth, M. Genest, J. Shaver and T. B. Mills: Int. J. Fatigue **29**

(a)

(b)

Fig. B·1   Log-log plot of scale a, horizontal axes, versus M_a, verical axes for the unfretted polished surfaces obtained from the image of Fig. 14. (a) in the vertical direction; (b) in the horizontal direction.

(2007) 810–821.
10) G. Frantziskonis and B. Loret: Eur. J. Mechanics **14** (1995) 873–892.
11) M. H. Jansen and P. J. Oonincx: *Second Generation Wavelets and Applications*, (Springer, 2003).
12) H. H. Szu: Wavelet Applications III, Proc. SPIE. **2762**, (Orlando, Florida, 2005).
13) J. M. Yang, C. N. Hwang, H. T. Chian and B. L. Yang: J. Taiwan Soc. Naval Architects Marine Eng. **26** (2007) 99–112.
14) T. Inoue, A. Sueoka, H. Kanemoto, S. Odahara and Y. Murakami: Key Eng. Mater. **347** (2007) 253–258.
15) P. Kumar and E. Foufoula-Georgiou: Rev. Geophysics **35** (1997) 385–412.
16) G. Frantziskonis and P. Deymier: Phys. Rev. B **68** (2003) 24105.
17) G. Frantziskonis, S. K. Mishra, S. Pannala, S. Simunovic, C. S. Daw, P. Nukala, R. O. Fox and P. A. Deymier: Int. J. Mult. Comp. Eng. **4** (2006) 755–770.
18) M. Ciavarella: Int. J. Solids Struct. **35** (1998) 2349–2362.
19) M. Ciavarella: Int. J. Solids Struct. **35** (1998) 2363–2378.
20) R. B. Waterhouse: RB Waterhouse and TC Lindley, ed. by Fretting fatigue, ESIS 18, (Mechanical Engineering Publications, London, 1994) 339–349.
21) T. E. Matikas and P. D. Nicolaou: J. Mater. Res. **16** (2001) 2716–2723.
22) T. Hattori and T. Watanabe: Tribology International **39** (2006) 1100–1105.
23) P. J. Golden and M. J. Shepard: Mater. Sci. Eng. A **468–470** (2007) 15–22.
24) E. Vanmarcke: Random Fields—Analysis and Synthesis, (Cambridge, Massachusetts, The MIT Press, 1983).
25) A. Yaglom: Correlation Theory of Stationary and Related Random Functions I: Basic Results, New York, Springer-Verlag, Inc. (1987).
26) I. Simonsen, A. Hansen and O. M. Nes: Phys. Rev. E **58** (1998) 2779–2787.